Dimyristoylphosphatidylcholine/C16:0-Ceramide Binary Liposomes Studied by Differential Scanning Calorimetry and Wide- and Small-Angle X-Ray Scattering

Juha M. Holopainen,* Jesper Lemmich,[†‡] Frank Richter,[§¶] Ole G. Mouritsen,[†] Gert Rapp,[§] and Paavo K. J. Kinnunen*

*Helsinki Biophysics and Biomembrane Group, Department of Medical Chemistry, Institute of Biomedicine, University of Helsinki, Helsinki, Finland; [†]Department of Chemistry, Technical University of Denmark, DK-2800 Lyngby, Denmark; [‡]Condensed Matter Physics and Chemistry Department, Risø, National Laboratory, DK-4000, Roskilde, Denmark; [§]European Molecular Biology Laboratory, Hamburg Outstation at DESY, D-22603 Hamburg, Germany; and [¶]Department of Physics, E22 Biophysics, TU Munich, 85748 Garching, Germany

ABSTRACT   Ceramide has recently been established as a central messenger in the signaling cascades controlling cell behavior. Physicochemical studies have revealed a strong tendency of this lipid toward phase separation in mixtures with phosphatidylcholines. The thermal phase behavior and structure of fully hydrated binary membranes composed of dimyristoylphosphatidylcholine (DMPC) and N-palmitoyl-ceramide (C16:0-ceramide, up to a mole fraction $X_{cer} = 0.35$) were resolved in further detail by high-sensitivity differential scanning calorimetry (DSC) and x-ray diffraction. Both methods reveal very strong hysteresis in the thermal phase behavior of ceramide-containing membranes. A partial phase diagram was constructed based on results from a combination of these two methods. DSC heating scans show that with increased X_{cer} the pretransition temperature T_p first increases, whereafter at $X_{cer} > 0.06$ it can no longer be resolved. The main transition enthalpy ΔH remains practically unaltered while its width increases significantly, and the upper phase boundary temperature of the mixture shifts to ~63°C at $X_{cer} = 0.30$. Upon cooling, profound phase separation is evident, and for all of the studied compositions there is an endotherm in the region close to the T_m for DMPC. At $X_{cer} \geq 0.03$ a second endotherm is evident at higher temperatures, starting at 32.1°C and reaching 54.6°C at $X_{cer} = 0.30$. X-ray small-angle reflection heating scans reveal a lamellar phase within the temperature range of 15–60°C, regardless of composition. The pretransition is observed up to $X_{cer} < 0.18$, together with an increase in T_p. In the gel phase the lamellar repeat distance d increases from ~61 Å at $X_{cer} = 0.03$, to 67 Å at $X_{cer} = 0.35$. In the fluid phase increasing X_{cer} from 0.06 to 0.35 augments d from 61 Å to 64 Å. An $L_{\beta'}/L_{\alpha}$ (ripple/fluid) phase coexistence region is observed at high temperatures (from 31 to 56.5°C) when $X_{cer} > 0.03$. With cooling from temperatures above 50°C we observe a slow increase in d as the coexistence region is entered. A sudden solidification into a metastable, modulated gel phase with high d values is observed for all compositions at ~24°C. The anomalous swelling for up to $X_{cer} = 0.30$ in the transition region is interpreted as an indication of bilayer softening and thermally reduced bending rigidity.

INTRODUCTION

The principal feature of cell membranes is the "fluid" lipid bilayer, which provides a barrier separating the cell interior from the surroundings. There is abundant evidence for lateral organization of cell membranes into domains with distinct lipid and protein compositions (Kinnunen, 1991). Detailed molecular-level mechanisms determining the organization of cell membranes have been studied extensively. Lipid domains and domain boundaries seem to be important for the activation of membrane-associating proteins such as protein kinase C (Hinderliter et al., 1997), cytochrome c (Mustonen et al., 1987), and the activity of phospholipase A_2 (Hønger et al., 1996), for instance. The lifetimes as well as the sizes of these domains vary and, as inferred from studies on model membranes, depend on the physical states and phase behavior of the constituent lipids (Mouritsen and Kinnunen, 1996).

Dimyristoylphosphatidylcholine (DMPC) (see Fig. 1 for chemical structure) bilayers are widely used as model membranes because of their well-characterized thermotropic behavior. This lipid exhibits two phase transitions, a pretransition at approx. $T_p = 14°C$ and the main transition at $T_m \approx 24°C$ (Silvius, 1982). Below T_m most of the acyl chains are in an all-*trans* configuration, and the bilayer is in the gel phase. At T_m, progressive *trans-gauche* isomerization results in lateral area expansion and decrease of bilayer thickness. The exact nature of this transition still remains incompletely understood. It has been suggested to involve a strongly fluctuating dynamic superlattice as an intermediate (Jutila and Kinnunen, 1997), which could be somewhat analogous to the liquid-ordered phase (Ipsen et al., 1990). Mixing DMPC with another lipid species can, in a similar way, provide lateral heterogeneity and modification of thermomechanic properties that can be suppressed or increased, depending on the molecular structure of the lipid added. The incorporation of, for instance, cholesterol into DMPC in increasing proportions results, at $X_{chol} < 0.04$, first in softening of the bilayer, whereas at $X_{chol} \geq 0.04$ an increase in membrane rigidity is observed (Lemmich et al., 1996).

Sphingolipids, with the exception of sphingomyelin, are normally minor components of cell membranes. In contrast

1,2-dimyristoyl-phosphatidylcholine (DMPC)

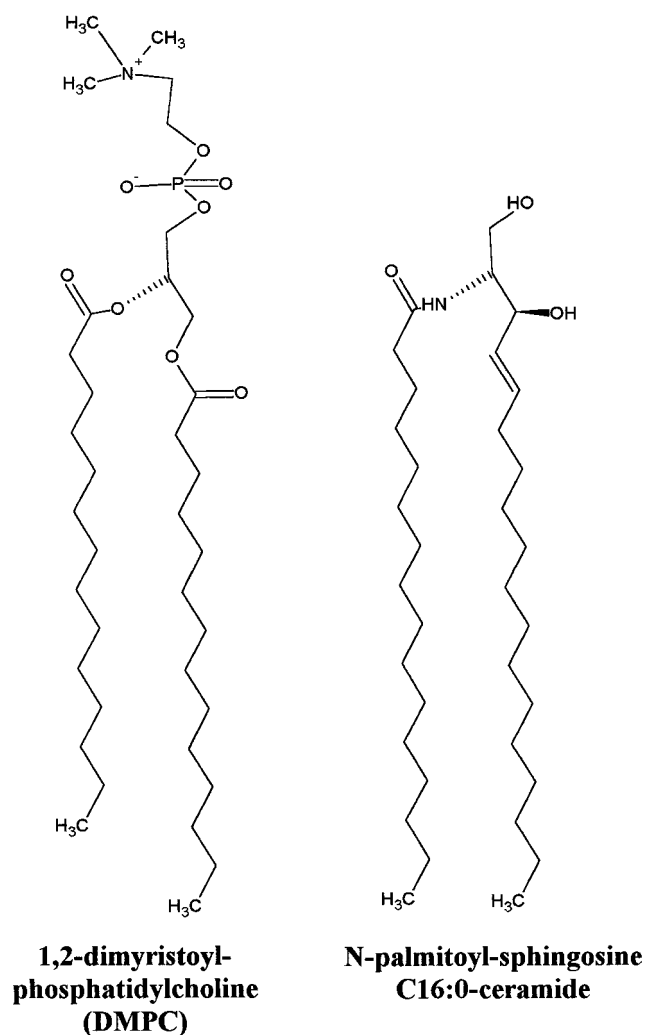**N-palmitoyl-sphingosine C16:0-ceramide**

FIGURE 1   Structures of DMPC and *N*-palmitoyl-sphingosine (C16:0-ceramide) used in this study.

to DMPC, their physical properties have received far less attention. Detailed understanding of the molecular level effects of ceramide (Fig. 1), for instance, on complex cellular membranes as well as on model biomembranes, remains elusive. Yet these data on these systems would be highly warranted, as ceramide has been identified as a central second messenger in cellular signaling cascades for differentiation, death, and senescence (Hannun and Obeid, 1995; Gómez-Muñoz, 1998). Ceramide is formed by the hydrolytic action of a specific enzyme, sphingomyelinase, on sphingomyelin (Hannun, 1994). Activation of sphingomyelinase has been suggested to result from agonist-induced activation of several receptors for tumor necrosis factor α, γ-interferon, and interleukin-1 (Hannun and Obeid, 1995; Liu and Anderson, 1995). The exact mechanisms of action of ceramide in the extracellular signal transduction from the plasma membrane into the cell, e.g., into its nucleus, are poorly understood. In keeping with the

amphiphilicity of lipids, it is essential to note that lipid-involving steps in signaling processes reside in membranes. Likewise, generation of these components changes the phase behavior and thus also the organization of the membranes accommodating them. The content of ceramide has been shown to reach up to 10 mol% of the total cellular lipids, and there is evidence for the accumulation of ceramide in specialized areas of the plasma membrane (Hannun, 1996; Liu and Anderson, 1995).

The amide group of ceramide is important for the conformation of the entire molecule, and a conical overall shape has been proposed (Pascher, 1976). The phase behavior of a fully hydrated *N*-hydroxy fatty acid ceramide from natural sources (HFA-Cer) as well as the corresponding non-hydroxy fatty acid ceramide (NFA-Cer) has been resolved (Han et al., 1995; Shah et al., 1995a,b). At 20°C HFA-Cer adopts a well-ordered multilamellar bilayer gel phase with a bilayer periodicity of 60.7 Å, with a wide-angle reflection at $1/(4.2 \text{ Å})$ that is typical for ordered chains. Increasing the temperature above the main transition at 91°C causes a transition into an inverted hexagonal (H_{II}) phase (Shah et al., 1995b). At 20°C fully hydrated NFA-Cer shows a well-ordered lamellar structure with a bilayer periodicity of 58.6 Å, with four wide-angle reflections with spacings of 4.6, 4.2, 4.0, and 3.8 Å. At 77°C the bilayer periodicity is reduced to 53.1 Å, and wide-angle reflections at $1/4.6$, $1/4.2$, and $1/3.8 \text{ Å}^{-1}$ are observed. Raising the temperature above T_m ($\sim$81°C) results in a single small-angle reflection positioned at $1/30.0 \text{ Å}^{-1}$, combined with a broad reflection centered at $1/4.6 \text{ Å}^{-1}$, thus indicating a molten chain phase. These results show that the NFA-Cer system displays a complex polymorphic phase behavior involving two gel phases. The same authors studied the behavior of synthetic C16:0-ceramide with the same techniques. Fully hydrated C16:0-ceramide displayed a broad exotherm at $\sim$50–70°C and an endothermic transition at 90.0°C (Shah et al., 1995a). X-ray diffraction showed that the exothermic reaction was accompanied by decreased bilayer periodicity and increased layer as well as chain-packing order. The endothermic transition was identified as the main transition involving a decrease in bilayer thickness, and a new diffuse reflection at 4.6 Å was observed, which is indicative of a melted chain phase.

Natural ceramides broaden and eventually eliminate the cooperative gel/liquid-crystalline phase transition of the host DMPC bilayer (Holopainen et al., 1997). Incorporation of ceramide from natural sources into DPPC increases the activity of phospholipase A_2 (Huang et al., 1997), which probably can be related to changes in the physical state of pure DPPC membranes undergoing phase transition (Hønger et al., 1996). Enzymatic formation of ceramide from sphingomyelin results in aggregation and partial fusion of liposomes (Ruiz-Argüello et al., 1996; Basáñez et al., 1997). We have shown natural ceramide to become enriched into microdomains, in both gel state and fluid

mixtures with DMPC (Holopainen et al., 1997). There is a large difference in a major portion of the sphingomyelin molecules in the sn-1 and sn-2 acyl chain lengths, and it has been shown that this distinction causes chain mismatch and lateral organization of the membrane (Bar et al., 1997). More specifically, whereas DMPC and *N*-palmitoyl-sphingomyelin (C16:0-SM) mix nearly ideally, *N*-lignoceryl-sphingomyelin (C24:0-SM) is immiscible with DMPC. While microdomain formation and demixing of natural ceramide with long *N*-acyl chains could result from hydrophobic mismatch (Lehtonen et al., 1996; Holopainen et al., 1997), our recent studies have revealed that the chain length difference is not the underlying mechanism (Holopainen et al., 1998). Accordingly, microdomain formation in fluid 1-palmitoyl-2-oleoyl-phosphatidylcholine (POPC) membranes could also be observed using C16:0-ceramide, with only minor hydrophobic mismatch. The observed microdomain formation in POPC was suggested to result from hydrogen bonding between the ceramide headgroups (Moore et al., 1997; Holopainen et al., 1998). In the present study x-ray diffraction of DMPC/C16:0-ceramide multilamellar vesicles was utilized to resolve structural changes caused by the latter lipid in these mixtures, while the enthalpies accompanying the transformation of the different thermotropic phases were measured by differential scanning calorimetry (DSC).

MATERIALS AND METHODS

Materials

HEPES, EDTA, and DMPC were purchased from Sigma, and C16:0-ceramide was from Northern Lipids (Vancouver, British Columbia, Canada). The purity of the above lipids was checked by thin-layer chromatography on silicic acid-coated plates (Merck, Darmstadt, Germany), using chloroform/methanol/water (65:25:4, v/v) for DMPC and 1,2-dichloroethane/methanol/water (90:20:0.5, v/v) as a solvent system for C16:0-ceramide. Examination of the plates after iodine staining revealed no impurities. Concentrations of the lipids were determined gravimetrically with a high-precision electrobalance (Cahn, Cerritos, CA).

Sample preparation

Appropriate amounts of the lipid stock solutions were mixed in chloroform to obtain the desired compositions. The resulting mixtures were then evaporated to dryness under a stream of nitrogen, and traces of solvent were subsequently removed by evacuation under reduced pressure for at least 12 h. When the dry residue was not used immediately it was stored at $-20°C$.

Differential scanning calorimetry

Differential heat capacity scans were recorded at a lipid concentration of 0.7 mM and at a heating rate of 0.5°C/min. The samples were hydrated at 80°C in 5 mM HEPES and 0.1 mM EDTA (pH 7.4) and thereafter sonicated for 2 min in a bath-type ultrasonicator (Ultrasonik 104H NEY, Yucaipa, CA). Before they were loaded into precooled DSC cuvettes, the samples were equilibrated on ice for ~24 h and were thereafter degassed

at low pressure. The calorimeter (VP-DSC; MicroCal, Northampton, MA) was interfaced to a PC, and data were analyzed using the routines of the software provided with the instrument. All samples were scanned by heating from 5°C to 85°C and held at 85°C for 60 min with subsequent cooling back to 5°C, at a cooling rate of 0.5°C/min. Recent experimental results have shown that the sample preparation method can have a profound influence on the mixing behavior of lipids (Buboltz and Feigenson, 1999; Huang et al., 1999; Thompson et al., 1985). To investigate the possibility that our results were due to the particular method used for dispersing the lipids, we hydrated the dried lipid film (for $X_{cer} = 0.21$ and 0.30) at 90°C for 30 min, which was then followed by extensive (20 times) freeze-thawing (at 95°C). Subsequently, these samples were kept on ice for 72 h before they were loaded into the DSC cuvettes. Results obtained with these liposomes were essentially identical to those obtained when the bath-type sonicator was used to facilitate lipid dispersion. In fact, the latter is routinely employed in sample preparation for x-ray scattering studies (Rapp et al., 1995; Rappolt and Rapp, 1996a,b).

X-ray diffraction

The samples for x-ray diffraction were prepared essentially as described for DSC experiments, with the exception that the concentration of lipid was 10 w/w % (~0.15 M). The time-resolved x-ray diffraction experiments were performed at beamline X13 of the EMBL outstation at DESY. In brief, the beamline comprises a monochromator-mirror arrangement with a triangular silicon monochromator for horizontal focusing and 12 planar quartz mirrors aligned on an aluminum bench for vertical focusing (for a detailed description, see Rapp, 1992). With this set-up the wavelength of the x-rays is 1.5 Å; higher harmonics are rejected by the mirrors. Sets of tungsten slits were used to adjust the beam size at the sample (~0.5 mm in height and ~2 mm in width) and to reduce parasitic scattering. One-dimensional diffraction patterns were recorded simultaneously in the small- and wide-angle regime, using two linear position-sensitive detectors connected in series (Rapp et al., 1995) The camera length was set at 277 cm. Excess radiation was avoided with a small solenoid driven shutter close to the sample. Additional information, like temperature, ring current, and x-ray flux measured with an ionization chamber in front of the sample, was stored in the local memory. The temperature was controlled by a Peltier element and monitored by a thermocouple positioned close to the sample. Approximately 20 μl of the lipid suspension was transferred into a capillary tube, which was then allowed to equilibrate at 10°C for ~0.5 h in the sample holder (Rappolt and Rapp, 1996a). The sample was subsequently heated at a scan rate of 1°C/min up to 70°C. During this temperature scan, diffraction data were recorded for 10 s every minute. Cooling scans were performed under the same conditions. The reciprocal spacings (s) and scattering vectors (q)

$$s = 1/d = (2/\lambda)\sin\theta$$

$$q = 2\pi s = (4\pi/\lambda)\sin\theta$$

(where d is the lattice spacing, 2θ is the scattering angle, and λ is the wavelength of radiation) were calibrated by the diffraction pattern of rat-tail collagen with a long spacing of 640 Å.

RESULTS

Representative DSC up- and downscans for DMPC/C16:0-ceramide multilamellar vesicles (MLVs) are illustrated in Fig. 2. Neat DMPC shows two transitions, a pretransition at 14.4°C and a main transition at 23.7°C, in accordance with published data (Silvius, 1982). Increasing X_{cer} to 0.03 causes T_p to shift first to 16.4°C and then to 15.3°C ($X_{cer} = $
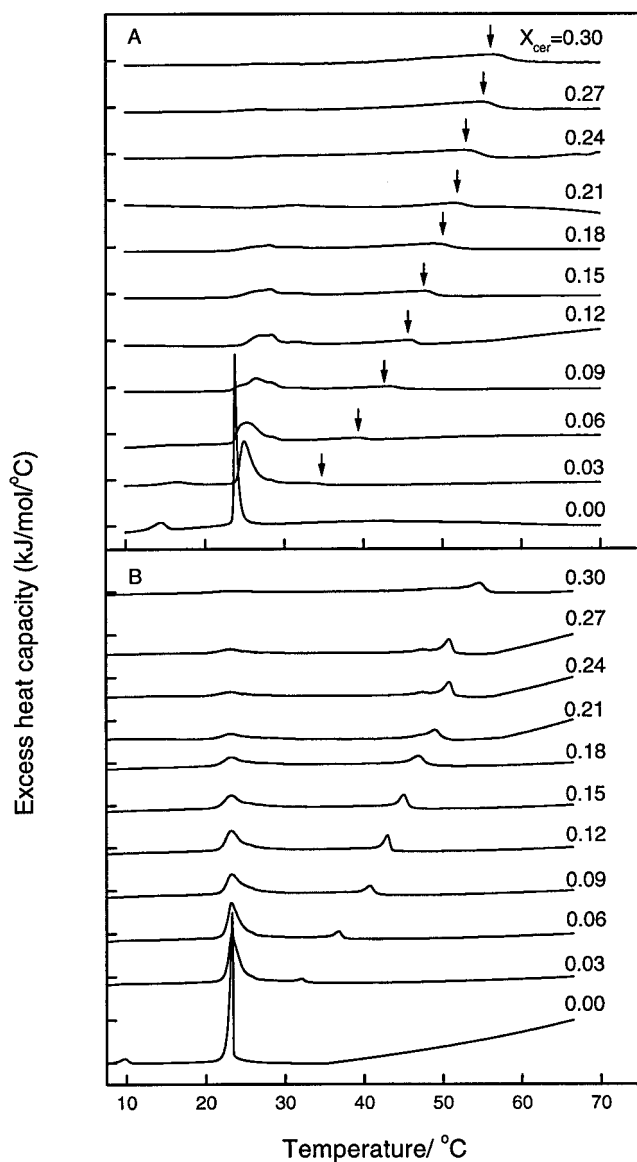
FIGURE 2 (*A*) High-sensitivity differential scanning calorimetry (DSC) heating scans for multilamellar DMPC/C16:0-ceramide vesicles (MLVs). The mole fraction of ceramide, X_{cer}, is indicated in the figure. The total lipid concentration was 0.7 mM in 5 mM HEPES, 0.1 mM EDTA (pH 7.4). (*B*) Data for the same MLVs recorded upon cooling. The arrow indicates the fourth endotherm (see also Fig. 3).
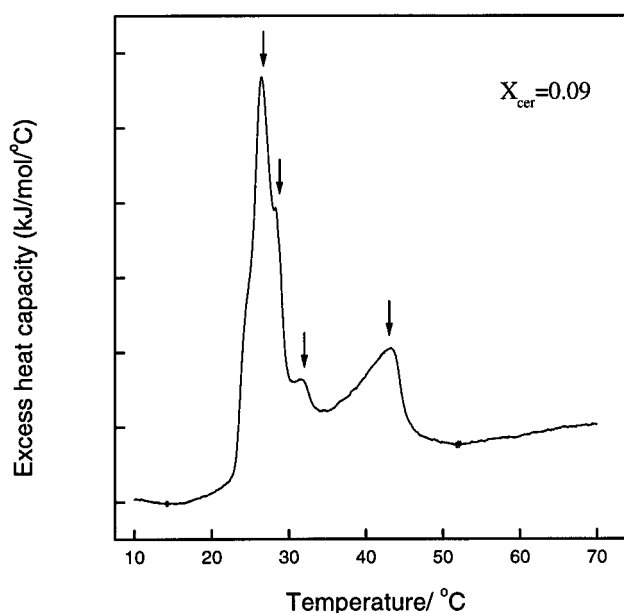

FIGURE 3 A high-resolution differential scanning calorimetry (DSC) heating scan for DMPC/C16:0-ceramide MLVs (molar ratio 91:9, respectively) showing the four distinct endotherm peaks.

56.5°C at X_{cer} = 0.30. In cooling scans for neat DMPC, the pretransition decreases by ~4.6°C compared to upscans and cannot be resolved from the DSC traces for MLVs containing ceramide. For neat DMPC, the main transition endotherm peak at 23.3°C (Fig. 4 *B*) remains at 23.1–23.7°C when X_{cer} is increased from 0.03 to 0.30. In contrast, with increasing X_{cer} the other clearly visible endotherm shifts from 32.1 to 54.6°C in a rather monotonic way (Fig. 4 *B*). In addition, when X_{cer} is varied from 0.24 to 0.30 a third endotherm can be resolved at a temperature around 47.5–49.3°C.

The intense aggregation observed for the samples with X_{cer} > 0.3 was problematic in the x-ray experiments, and only weak signals could be observed. Accordingly, we will focus on data collected at X_{cer} ≤ 0.35. Fig. 5 displays a selection of small-angle (SAXS, Fig. 5, *traces a–e*) and wide-angle (WAXS, Fig. 5, *traces f–j*) x-ray diffraction patterns at X_{cer} = 0.06, 0.12, 0.18, 0.24, and 0.30, recorded during heating. Every fifth pattern recorded is depicted (i.e., ΔT = 5° between subsequent patterns), starting at 15°C and ending at 60°C (50°C for X_{cer} = 0.12). In all cases the SAXS patterns are consistent with lamellar phases. Because of the limited q-region probed, only the first two orders of diffraction were observed. In some cases the peaks are very broad, and split into two, typical for the coexistence of two lamellar phases. In the WAXS pattern a single peak is observed at the lower temperatures. This peak stems from the ordering of the lipid chains and is observed whenever an $L_{\beta'}$ or $P_{\beta'}$ phase is present. The upper phase boundary of a gel-fluid coexistence region can thus be directly determined
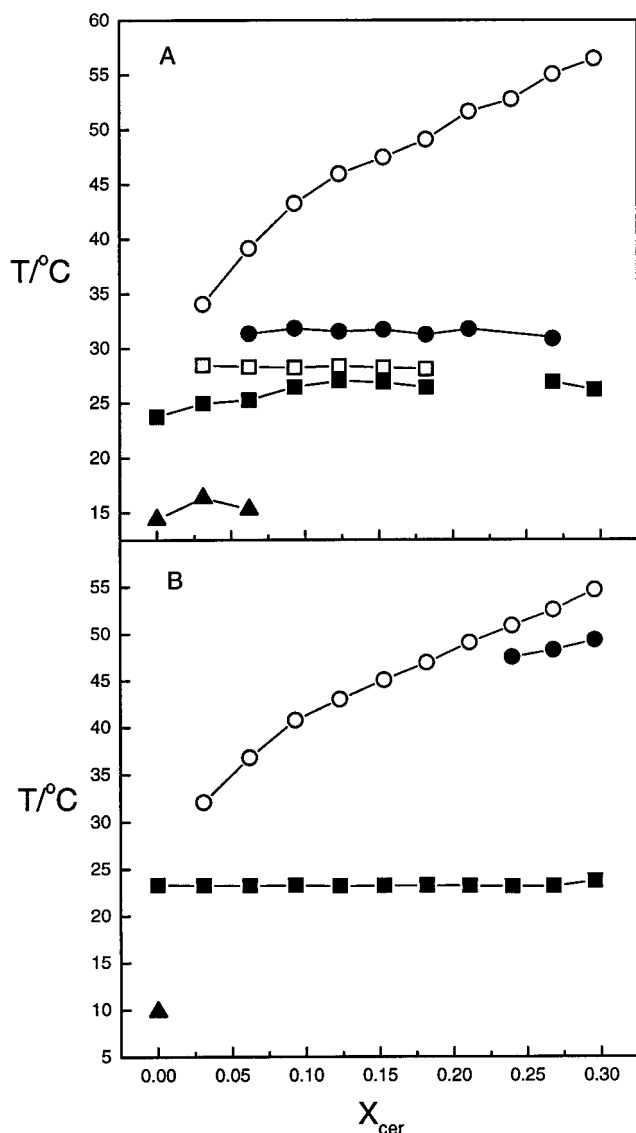
0.06) (not observable in Fig. 2), whereafter at increasing content of ceramide this transition could no longer be resolved. The main transition is broadened by ceramide, and already at X_{cer} = 0.06 (not observable in the plot) four peaks are observed (see Fig. 3 for a higher magnification of X_{cer} = 0.09, showing the four endotherm peaks). While the endotherm at ~23.7°C remains at about the same temperature, new endotherms appear at ~28.2–28.5 (X_{cer} = 0.03–0.18) and 30.8–31.7°C (X_{cer} = 0.06 to 0.27). The fourth endotherm (Fig. 4 *A*; marked with an *arrow* in Fig. 2 *A*) is progressively shifted to higher temperatures, reaching

FIGURE 4 Endotherm peak temperatures resolved during heating (*A*) and cooling (*B*) scans for DMPC/C16:0-ceramide MLVs as a function of ceramide content, X_{cer}.

from the WAXS pattern. The patterns observed at the lowest temperature used are consistent with the $L_{\beta'}$ gel phase, whereas the patterns observed at the higher temperatures reveal a fluid L_{α} phase.

From the DSC scans, we know that the $P_{\beta'}$ phase should be present up to $X_{cer} \leq 0.06$. In Fig. 5, *a* and *b*, the patterns taken for $X_{cer} = 0.06$ and 0.12 at 20 and 25°C are in keeping with the presence of a $P_{\beta'}$ phase (i.e., asymmetrical peaks due to the ripples). However, it is difficult to distinguish between regions where either a pure $P_{\beta'}$ ripple phase or $P_{\beta'}$ coexisting with the $L_{\beta'}$ and L_{α} phases is present. Phase coexistence is observed at higher temperatures, and for X_{cer} = 0.12–0.27, splitting of the second-order peaks into two can be observed, indicating that there must be rather large coexisting domains of the two phases.

At $X_{cer} > 0.18$ the peaks typical for $P_{\beta'}$ are no longer visible (Fig. 5). Instead, there is a very broad gel-fluid coexistence region, and increased splitting of the second-order peaks is observed. The patterns recorded at X_{cer} = 0.15 and 0.21 display the same features. At $X_{cer} = 0.24$ (and $X_{cer} = 0.27$) a similar behavior is observed, yet both the SAXS and WAXS patterns display much sharper reflections than seen at lower ceramide contents. This indicates a larger correlation length in the gel phase domains of the lipids. Increasing $X_{cer} \geq 0.30$ causes the splitting of the peaks to disappear in the coexistence region, and in contrast to observations at lower contents of ceramide, the peaks are relatively sharp. The second-order peak displays a minimum in the q value, at 35°C, corresponding to a maximum in repeat distance (Fig. 5 *e*).

A detailed analysis of the position of the peaks in the SAXS pattern yields the repeat distance d. This has been done by fitting the first-order peaks to Lorentzian functions, i.e., $I(q) = I_0 + \alpha/[1+(q - q_1)^2\zeta^2]$ and $d = 2\pi/q_1$, where ζ is the correlation length, α is the prefactor, and I_0 denotes the incoherent background arising from the sample. The resulting Bragg peak is denoted by q_1. To a first approximation, we have neglected the fact that "double peaks" are observed in the coexistence region for X_{cer} = 0.12–0.27 (see below). The resulting repeat distances as a function of T and X_{cer}, determined from heating scans, are shown in Fig. 6. Starting at $X_{cer} = 0.03$, d increases from around 61 Å in the $L_{\beta'}$ phase to around 68 Å in the $P_{\beta'}$ phase (around 19–24°C). This is followed by a very narrow $P_{\beta'}$ and L_{α} phase coexistence region (around 24–27°C), whereafter d decreases monotonically to ~62 Å, as the L_{α} phase is entered. Except for the narrow coexistence region, this behavior is similar to that observed for pure DMPC. A similar behavior can be observed for $X_{cer} = 0.06$, 0.09, and 0.12. Yet, as X_{cer} increases, T_p also increases. Concomitantly, the region with pure $P_{\beta'}$ phase becomes narrow, whereas the coexistence region broadens. Even though a pretransition cannot be observed in the DSC experiments, a $P_{\beta'}$ phase can still be detected at $X_{cer} = 0.15$ and 0.18 in the x-ray data. However, as can be seen in Fig. 6, the amplitude of the modulation is decreasing, leading to smaller values of d. A second maximum in the repeat distance starts to grow within the coexistence region, already at $X_{cer} = 0.12$. This is likely to be a purely kinetic effect due to the growth of fluid domains in the gel matrix. The maximum in d can be attributed to an entropic repulsion due to a softening of the bilayer. We shall return to this point later. At high values of X_{cer}, the characteristic bend in the d spacing curves marks the termination of the two-phase region.

Fig. 7 displays d spacings determined during cooling scans for $X_{cer} = 0.06$, 0.15, 0.21, 0.24, 0.27, and 0.32. These data are clearly different from those determined from heating scans depicted in Fig. 6 above. The main reason for this is that the kinetics of formation of the gel phases is very slow. Starting at high temperatures, we observe a slow

FIGURE 5 X-ray diffraction pattern for DMPC, incorporating varying contents of C16:0-ceramide, X_{cer}. (a–e) SAXS; (f–j) WAXS. The mole fraction of ceramide, X_{cer}, is indicated in the figure. The patterns were recorded during heating. The temperature difference between consecutive patterns is 5°.
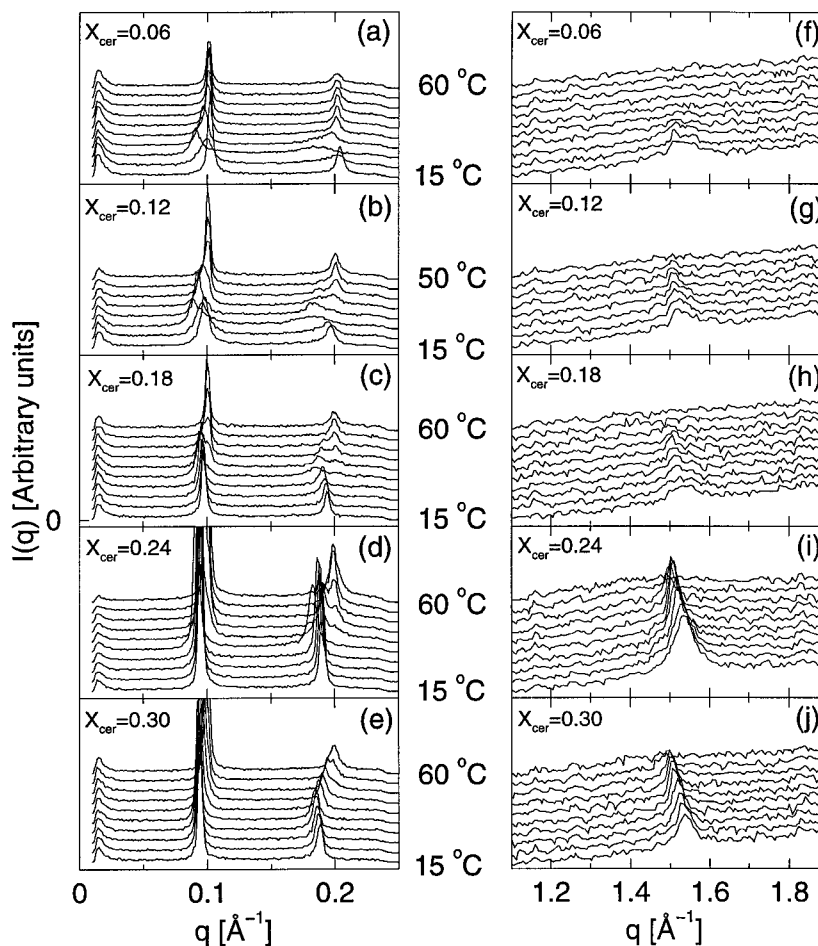
increase in d spacing when the temperature is lowered into the coexistence region. In part of the coexistence region it is possible to observe a splitting of the second-order peak. A sudden solidification into a metastable, probably modulated gel phase with a large repeat distance is in all cases observed at $T = 24°C$, corresponding to T_m for pure DMPC. This complex kinetic effect is well documented and has previously been described for pure DPPC (Rappolt and Rapp, 1996b). In brief, during cooling from L_α and entering the metastable $P_{\beta'}$ phase, the water content is ~30% higher compared to the stable $P_{\beta'}$ phase and is thus even higher than in the liquid crystalline phase for DPPC. The nonequilibrium behavior of the system during downscans is consistent with the DSC data. Here, essentially only two peaks are observed, one at high temperature, denoting the upper phase boundary, and one at around $T = 24°C$, denoting the sudden solidification process.

DISCUSSION

In the present paper we address properties of phospholipid/ceramide mixtures by using DMPC and the well-defined synthetic C16:0-ceramide. It has been shown that the struc-

turally closely related sphingomyelin, having the phosphocholine group esterified to ceramide, is miscible in PC membranes as long as there is no hydrophobic mismatch and the T_m's do not differ too much (Calhoun and Shipley, 1979; McElhaney, 1982; McKeone et al., 1986; Bar et al., 1997). The first three carbons (C1-C3) of sphingosine backbone of sphingomyelin are structurally equivalent to the three glycerol carbons of glycerophospholipids such as PC, while C4 is more or less equivalent to the sn-1 esterbond oxygen of PC. In keeping with the above, C16:0-ceramide, having a saturated C16 hydrocarbon chain and a C16:0 esterified at the NH_2 group, is sterically very close to DMPC, which has saturated C14:0 chains, and should therefore match a DMPC bilayer with regard to its hydrophobic length.

A phase diagram constructed from the x-ray and DSC data recorded during upscans is displayed in Fig. 8. As not all phase boundaries could be determined accurately from the present results, some approximation was necessary. Yet it should be emphasized that the phase behavior of the DMPC/C16:0-ceramide mixture is very complex, as clearly seen in Fig. 3. Accordingly, the phase diagram shown represents the simplest one consistent with our data. In DSC
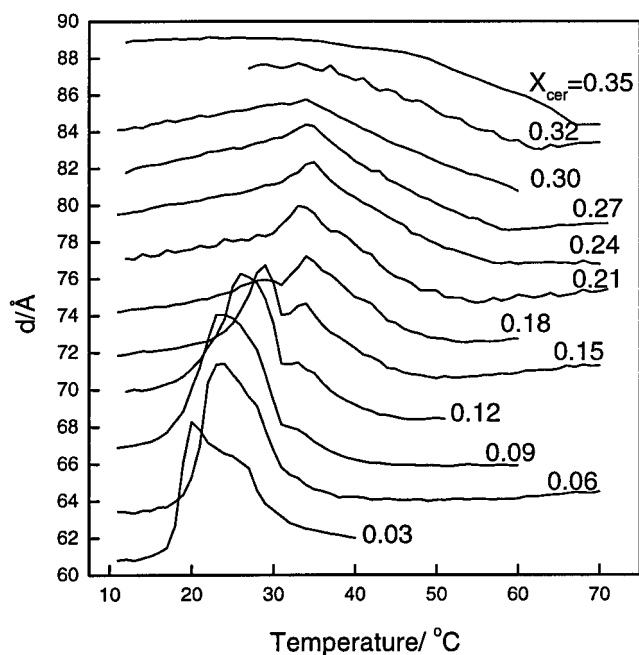
FIGURE 6 Lamellar repeat distance d for DMPC with varying contents, X_{cer}, of C16:0-ceramide (X_{cer} = 0.03–0.35, indicated in the figure), as determined from single Lorentzian fits to SAXS patterns recorded during heating scans. See text for details. For the sake of clarity, each data set above that for X_{cer} = 0.03 has been displaced by 2.0 Å relative to that below.

FIGURE 7 Lamellar repeat distance d for DMPC containing increasing amounts of C16:0-ceramide, X_{cer} (indicated in the figure), as determined from single Lorentzian fits to SAXS patterns recorded during cooling scans. For the sake of clarity, each data set above that for X_{cer} = 0.06 has been displaced by 2.0 Å relative to that below.

scans at X_{cer} = 0.03 a significantly broader peak is evident, with two additional smaller peaks and an additional pretransition peak, indicating a narrow phase coexistence region between the $P_{\beta'}$ phase and the L_{α} phase. As X_{cer} is increased to 0.06 a clear second peak is observed, and at still higher ceramide contents four peaks are observed in the DSC scans. The upper peak is quite distinct and is relatively constant at a temperature around T = 31°C. This is consistent with the point from x-ray scattering, where there is a bend in the d spacing curves for X_{cer} = 0.09, 0.12, 0.15, and 0.18 above the peak, arising from the $P_{\beta'}$ phase, and with the point where the d spacing starts to increase rapidly for the membranes with higher contents of ceramide. Thus we have a horizontal line at T = 31°C and $X_{cer} \approx$ 0.06, which determines the beginning of an $L_{\beta'}/L_{\alpha}$ phase coexistence region. The existence of such a line is in keeping with the distinct peak observed in the DSC scans, revealing the melting process to involve a large enthalpy change. The upper phase boundary of the $L_{\beta'}/L_{\alpha}$ phase coexistence region (and the $P_{\beta'}/L_{\alpha}$ phase coexistence region up to $X_{cer} \approx$ 0.06) can be determined independently and quite accurately from the DSC scans and from the WAXS pattern, as described above. The values determined from the data obtained by these two methods are in good agreement. Below the horizontal line in the phase diagram, thermodynamics dictates that there must be a coexistence between two gel phases (not shown in Fig. 8). Because the $P_{\beta'}$ phase is only
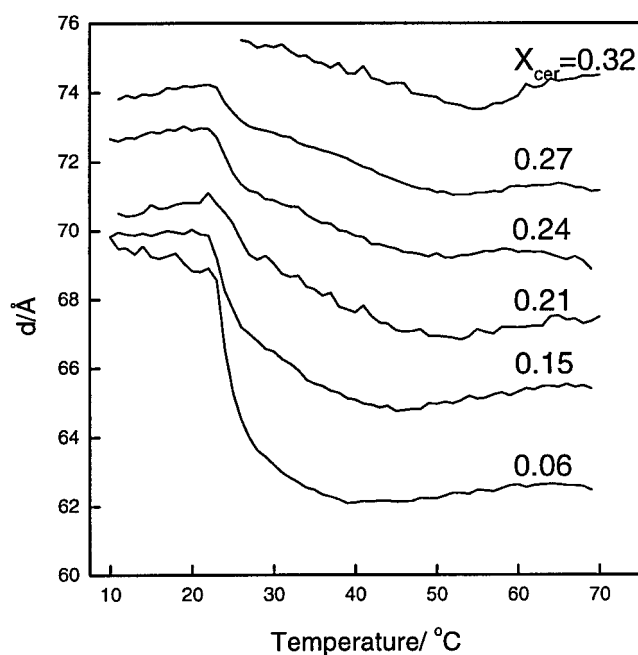
observed up to X_{cer} = 0.18, there must be a point between X_{cer} = 0.18 and X_{cer} = 0.21, where the lower $L_{\beta'}/L_{\alpha}$ coexistence line starts to ascend from 31°C. At higher ceramide contents, we probably have an $L_{\beta'}$ phase in coex-
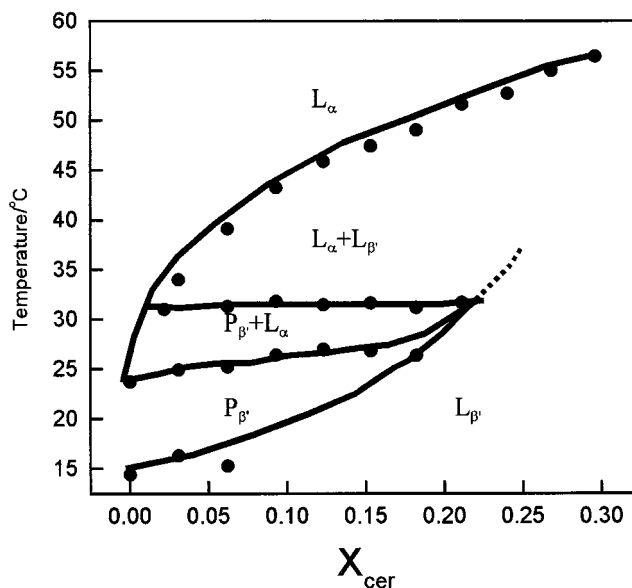

FIGURE 8 Phase diagram for DMPC with C16:0-ceramide up to X_{cer} = 0.30. See text for details. The lines connecting measured data points represent guides to the eye.

istence with another ceramide-rich L_β phase. In regions where phase transformations between different gel phases take place (i.e., $L_{\beta'} \rightarrow P_{\beta'}$), one would rather observe a broad signal than distinct peaks in the DSC scans. It is therefore not possible to determine the position of the phase boundaries precisely. Because T_m for pure C16:0-ceramide is around 80–90°C (Shah et al., 1995a), a possible scenario for the remaining part of the phase diagram could be that the horizontal phase boundary at $T = 31$°C starts to bend upward for higher ceramide contents, so that the $L_{\beta'}/L_\alpha$ phase coexistence envelope will close up at $T = 80$–90°C for pure ceramide and give rise to a pure L_β phase at lower temperatures. Interestingly, a dipalmitoylphosphatidylcholine (DPPC)/dipalmitoylphosphatidylethanolamine (DPPE) phase diagram (Blume et al., 1982) resembles the one described in this paper, in keeping with the small, weakly hydrated headgroup and a comparatively large hydrocarbon chain volume of PE.

Unfortunately, a quantitative description of the different phases observed is somewhat limited, as only two diffraction orders can be observed in the x-ray data, thus limiting the information to the values for d spacings versus X_{cer}. The repeat distances d measured during upscans for $T = 12$°C, representing a pure $L_{\beta'}$ phase, and for $T = 60$°C, representing a pure L_α phase (with the exception of $X_{cer} = 0.35$, just below the phase boundary) are compiled in Fig. 9. At $X_{cer} = 0.03$ the d spacing is 61 Å in the $L_{\beta'}$ phase, which corresponds reasonably well to the value observed for pure DMPC. With increasing ceramide contents, the d spacing
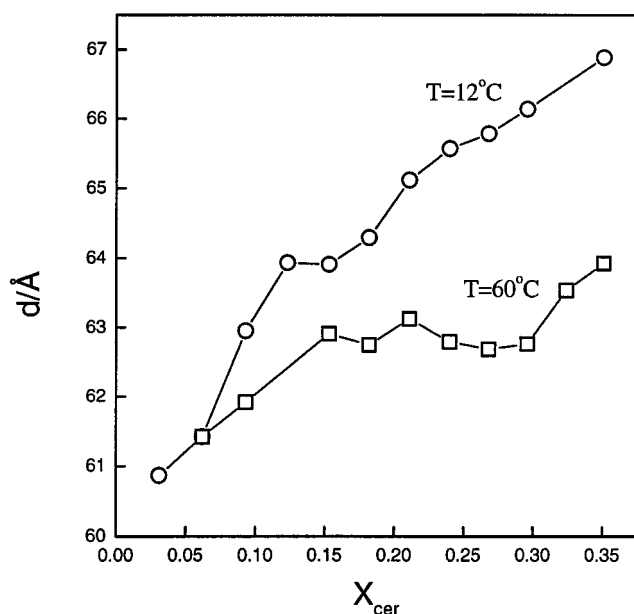
increases monotonically up to 67 Å. This 6 Å increment is in keeping with the increase one would expect if the acyl chains were no longer tilted. Accordingly, upon the addition of C16:0-ceramide the $L_{\beta'}$ phase would gradually be transformed into an untilted L_β phase. This effect is easily explained as follows. First, the tilt in the $L_{\beta'}$ phase for pure DMPC results from the excess area of the headgroups relative to the acyl chains. Because C16:0-ceramide is characterized by a small headgroup area, relative to the acyl chains (in contrast to DMPC), the tilting of DMPC becomes unnecessary when sufficient amounts of C16:0-ceramide are included. Second, the acyl chains of the C16:0-ceramide molecules contain two carbon atoms more than DMPC, resulting in a small increase in the bilayer thickness. In the L_α phase we also observe an increase in the d spacing from 61 Å at $X_{cer} = 0.06$ to 64 Å at $X_{cer} = 0.35$, which is compatible with the length difference between DMPC and C16:0-ceramide.

The kinetic effects observed in the $L_{\beta'}/L_\alpha$ phase coexistence region are of interest and are readily evident upon examination of the data collected at $X_{cer} = 0.24$, for instance. The d spacings determined during both up- and downscans are shown in Fig. 10. In both cases, there are regions where the second-order peaks can be dissolved into two distinct peaks, as described above. In these cases we have displayed the two coexisting d spacings, d_1 and d_2, determined from double Lorentzian fits to the second-order peaks. In the coexistence region there is a significant dif-
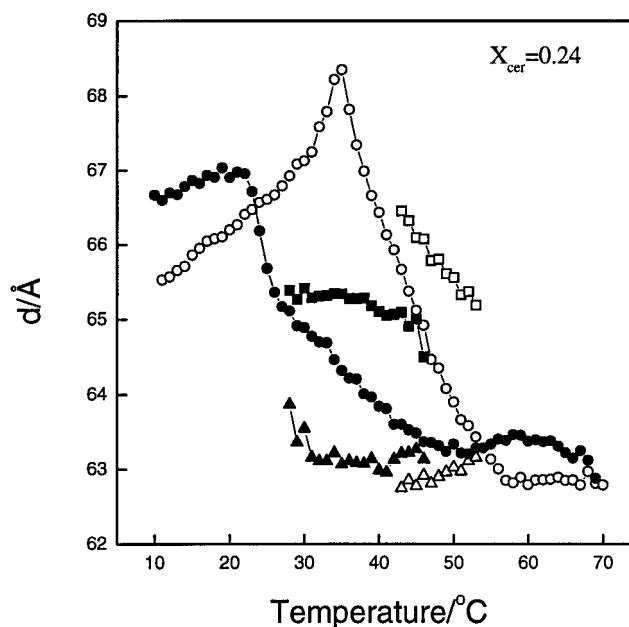

FIGURE 9 Lamellar repeat distance d for DMPC at varying ceramide content, X_{cer}, as determined from single Lorentzian fits to SAXS patterns recorded during heating scans displayed at fixed temperatures of $T = 12$°C (○), corresponding to the $L_{\beta'}$ phase, and $T = 60$°C (□), corresponding to the L_α phase.

FIGURE 10 Lamellar repeat distance d for DMPC at $X_{cer} = 0.24$ (○), as determined from Lorentzian fits. Where two distinct peaks could be resolved, a double Lorentzian fit to the second-order peak was performed, resulting in two repeat distances, d_1 (□) and d_2 (△). Open and closed symbols denote data for heating and cooling scans, respectively.

ference between the d spacings determined during upscans and downscans. During the downscans, when the phase coexistence region is entered from above, the d spacing increases monotonically. From $T = 46°C$ down to $28°C$, distinct $L_{\beta'}$ and L_α domains can be resolved. The values for d_1 around 65 Å correspond rather well to the d spacings observed for a pure $L_{\beta'}$ phase (cf. Fig. 10) at $X_{cer} = 0.24$, whereas the values of d_2 seem to be in reasonable agreement with the plateau of the d spacings in the L_α phase. In contrast, we observe that d starts to increase dramatically when the phase coexistence region is entered at $T = 31°C$ during the upscan, the maximum value for d being reached at $T = 35°C$. After that a rapid decrease is observed, and in the range from 43 up to $53°C$ distinct L_α and $L_{\beta'}$ domains can be observed. The peak in d can be explained as a kinetic effect resulting from the growth of the L_α phase in the $L_{\beta'}$ matrix. The scan rate, $1°$/min, is rather fast compared to the kinetics involved in the phase separation process in binary lipid mixtures in the coexistence region (Jørgensen et al., 1996). We can thus expect that as the phase coexistence region is reached at $T = 31°C$, only small isolated patches of fluid domains will form in the gel matrix. After a while, these domains start to connect, and around $T = 35°C$ we probably have a percolating structure of gel and fluid domains (e.g., Weis and McConnell, 1985; Weis, 1991). This will give rise to heterogeneity and strong compositional fluctuations on a very small length scale (microheterogeneity). When these fluctuations couple with the out-of-plane motions of the bilayers, a lowering of the bending rigidity can result, which in turn can lead to an increase in the repulsive undulation forces between the bilayers, thus increasing the d spacing (Helfrich, 1978). When the maximum value of d has been reached, the domains grow in size, and d decreases again. Thus the peak observed in the d spacing would be similar in origin to the anomalous swelling effect observed for pure DMPC bilayers in the region close to T_m (Hønger et al., 1994).

Based on several lines of research, ceramide has been classified as a lipid second messenger in cellular signaling cascades for apoptosis, endocytosis, cell differentiation, growth, and cell senescence (Hannun, 1996; Gómez-Muñoz, 1998). Perhaps the best characterized example of bioactive lipids is platelet-activating factor (PAF). Accordingly, concentrations of PAF as low as 10^{-10} M are sufficient to elicit its biological responses (e.g., Voet and Voet, 1995), and a specific plasma membrane receptor belonging to the family with seven transmembrane helices and coupled to G-proteins has been described (e.g., Chao and Olson, 1993; Izumi and Shimizu, 1995). In contrast, stimulation of cells by heat or radiation, for instance, to induce apoptosis has been reported to produce ceramide up to 10 mol% of the total phospholipid, corresponding to tens of nanomoles of ceramide (Hannun, 1996). Interestingly, during apoptosis it seems that the signal to cell death derives from C16:0-ceramide and that only minor elevations in other ceramide

species are observed (Thomas et al., 1999). In line with the above, understanding of the phase behavior of these systems is highly warranted. Our previous studies (Holopainen et al., 1997, 1998, 2000) and the constructed phase diagram (Fig. 8) reveal that even low contents of ceramide segregate into gel-state microdomains in both gel and fluid membranes and at physiological temperature. In cellular membranes ceramide is formed from sphingomyelin that is miscible and fluid at physiological temperatures in PC membranes. Accordingly, the formation of gel-like domains by ceramide should have a major impact on the overall physical state and organization of cellular membranes. We have recently demonstrated the formation of ceramide-enriched microdomains in fluid liposomes composed of sphingomyelin and phosphatidylcholine following the action of sphingomyelinase (Holopainen et al., 1998). With the use of giant liposomes this segregation of the ceramide formed by sphingomyelinase could be visualized by fluorescence microscopy (Holopainen et al., 2000). Moreover, these domains with enriched ceramide separate from the membrane as smaller vesicles in a vectorial manner, i.e., into the space opposite the site of action of sphingomyelinase. Accordingly, generation of ceramide can influence both two- as well as three-dimensional organization of membranes, resulting in altered microcompartmentalization in cells. There is evidence for the localization of a range of plasma membrane receptors with specific domains called caveolae (Smart et al., 1999). These specialized regions of the plasma membrane have been reported to contain ceramide (Liu and Anderson, 1995). The massive formation of ceramide observed in apoptosis could thus serve several functions, as follows. First, it would make the plasma membrane mechanically resistant and less permeable, similar to the function assigned to ceramide in skin, where this lipid is thought to provide the key element in the permeability barrier (Elias and Menon, 1991). Second, ceramide-induced segregation and compartmentalization of signaling molecules would make cells unresponsive to extracellular signals. Accordingly, it may well be necessary to revise the paradigm of lipid second messengers, mediating their downstream effects by interactions as monomers with specific receptor and effector proteins.

REFERENCES

Bar, L. K., Y. Barenholz, and T. E. Thompson. 1997. Effect of sphingo-myelin composition on the phase structure of phosphatidylcholine-sphingomyelin bilayers. *Biochemistry.* 36:2507–2516.

Basáñez, G., M. B. Ruiz-Argüello, A. Alonso, F. M. Goñi, G. Karlsson, and K. Edwards. 1997. Morphological changes induced by phospho-lipase C and by sphingomyelinase on large unilamellar vesicles: a cryo-transmission electron microscopy study of liposome fusion. *Biophys. J.* 72:2630–2637.

Blume, A., R. J. Wittebort, S. K. Das Gupta, and R. G. Griffin. 1982. Phase equilibria, molecular conformation, and dynamics in phosphatidylcholine/phosphatidylethanolamine bilayers. *Biochemistry.* 21:6243–6253.

Buboltz, J. T., and G. W. Feigenson. 1999. A novel strategy for the preparation of liposomes: rapid solvent exchange. *Biochim. Biophys. Acta.* 1417:232–245.

Calhoun, W. I., and G. G. Shipley. 1979. Sphingomyelin-lecithin bilayers and their interaction with cholesterol. *Biochemistry.* 18:1717–1722.

Chao, W., and M. S. Olson. 1993. Platelet activating factor: receptors and signal transduction. *Biochem. J.* 292:617–629.

Elias, P. M., and G. K. Menon. 1991. Structural and lipid biochemical correlates of the epidermal permeability barrier. *Adv. Lipid Res.* 24:1–26.

Gómez-Muñoz, A. 1998. Modulation of cell signalling by ceramides. *Biochim. Biophys. Acta.* 1391:92–109.

Han, C. H., R. Sanftleben, and T. S. Wiedmann. 1995. Phase properties of mixtures of ceramides. *Lipids.* 30:121–128.

Hannun, Y. A. 1994. The sphingomyelin cycle and the second messenger function of ceramide. *J. Biol. Chem.* 269:3125–3128.

Hannun, Y. A. 1996. Functions of ceramide in coordinating cellular responses to stress. *Science.* 274:1855–1859.

Hannun, Y. A., and L. M. Obeid. 1995. Ceramide: an intracellular signal for apoptosis. *Trends Biol. Sci.* 20:73–77.

Helfrich, W. 1978. Steric interactions of fluid membranes in multilayer systems. *Z. Naturforsch.* 33a:305–315.

Hinderliter, A. K., A. R. G. Dibble, R. L. Biltonen, and J. J. Sando. 1997. Activation of protein kinase C by coexisting diacylglycerol-enriched and diacylglycerol-poor lipid domains. *Biochemistry.* 36:6141–6148.

Holopainen, J. M., M. I. Angelova, and P. K. J. Kinnunen. 2000. Vectorial budding of vesicles by asymmetric enzymatic formation of ceramide in giant liposomes. *Biophys. J.* 78:830–838.

Holopainen, J. M., J. Y. A. Lehtonen, and P. K. J. Kinnunen. 1997. Lipid microdomains in dimyristoylphosphatidylcholine-ceramide liposomes. *Chem. Phys. Lipids.* 88:1–13.

Holopainen, J. M., M. Subramanian, and P. K. J. Kinnunen. 1998. Sphingomyelinase induced lipid microdomain formation in a fluid phosphatidylcholine/sphingomyelin membrane. *Biochemistry.* 37:17562–17570.

Hønger, T., K. Jørgensen, R. L. Biltonen, and O. G. Mouritsen. 1996. Systematic relationship between phospholipase A$_2$ activity and dynamic lipid bilayer microheterogeneity. *Biochemistry.* 35:9003–9006.

Hønger, T., K. Mortensen, J. H. Ipsen, J. Lemmich, R. Bauer, and O. G. Mouritsen. 1994. Anomalous swelling of multilamellar lipid bilayers in the transition region by renormalization of curvature elasticity. *Phys. Rev. Lett.* 72:3911–3914.

Huang, H.-W., E. M. Goldberg, and R. Zidovetski. 1997. Ceramide induces structural defects into phosphatidylcholine bilayers and activates phospholipase A$_2$. *Biochem. Biophys. Res. Commun.* 222:834–838.

Huang, J., J. T. Buboltz, and G. W. Feigenson. 1999. Maximum solubility of cholesterol in phosphatidylcholine and phosphatidylethanolamine bilayers. *Biochim. Biophys. Acta.* 1417:89–100.

Ipsen, J. H., K. Jørgensen, and O. G. Mouritsen. 1990. Density fluctuations in saturated phospholipid bilayers increase as the chain-length decreases. *Biophys. J.* 58:1099–1107.

Izumi, T., and T. Shimizu. 1995. Platelet-activating factor receptor: gene expression and signal transduction. *Biochim. Biophys. Acta.* 1259:317–333.

Jørgensen, K., A. Klinger, M. Braiman, and R. L. Biltonen. 1996. Slow nonequilibrium dynamical rearrangement of the lateral structure of a lipid membrane. *J. Phys. Chem* 100:2766–2769.

Jutila, A., and P. K. J. Kinnunen. 1997. Novel features of the main transition of dimyristoylphosphocholine bilayers revealed by fluorescence spectroscopy. *J. Phys. Chem. B.* 101:7635–7640.

Kinnunen, P. K. J. 1991. On the principles of functional ordering in biological membranes. *Chem. Phys. Lipids.* 57:375–399.

Lehtonen, J. Y. A., J. M. Holopainen, and P. K. J. Kinnunen. 1996. Evidence for the formation of microdomains in liquid crystalline large unilamellar vesicles caused by hydrophobic mismatch of the constituent phospholipids. *Biophys. J.* 70:1753–1760.

Lemmich, J., T. Hønger, K. Mortensen, J. H. Ipsen, R. Bauer, and O. G. Mouritsen. 1996. Solutes in small amounts provide for lipid-bilayer softness: cholesterol, short-chain lipids, and bola lipids. *Eur. Biophys. J.* 25:61–65.

Liu, P., and R. G. Anderson. 1995. Compartmentalized production of ceramide at the cell surface. *J. Biol. Chem.* 270:27179–27185.

McElhaney, R. N. 1982. The use of differential scanning calorimetry and differential thermal analysis of model and biological membranes. *Chem. Phys. Lipids.* 30:229–259.

McKeone, B. J., H. J. Pownall, and J. B. Massey. 1986. Ether phosphatidylcholines: comparison of miscibility with ester phosphatidylcholines and sphingomyelin, vesicle fusion, and association with apolipoprotein A-I. *Biochemistry.* 25:7711–7716.

Moore, D. J., M. E. Rerek, and R. Mendelsohn. 1997. FTIR spectroscopy studies of the conformational order and phase behaviour of ceramides. *J. Phys. Chem. B.* 101:8933–8940.

Mouritsen, O. G., and P. K. J. Kinnunen. 1996. Role of lipid organization and dynamics for membrane functionality. *In* Biological Membranes. K. Merz and B. Roux, editors. Birkhäuser, Boston. 463–502.

Mustonen, P., J. A. Virtanen, P. J. Somerharju, and P. K. J. Kinnunen. 1987. Binding of cytochrome *c* to liposomes as revealed by the quenching of fluorescence from pyrene-labeled phospholipids. *Biochemistry.* 26:2991–2997.

Pascher, I. 1976. Molecular arrangements in sphingolipids. Conformation and hydrogen bonding of ceramide and their implication on membrane stability and permeability. *Biochim. Biophys. Acta.* 455:433–451.

Rapp, G. 1992. Time-resolved x-ray diffraction studies on biological systems. *Acta Phys. Pol.* A82:103–120.

Rapp, G., A. Gabriel, M. Dosiere, and M. H. J. Koch. 1995. A dual detector single readout system for simultaneous small- (SAXS) and wide-angle (WAXS) scattering. *Nucl. Instrum. Methods A.* 357:178–182

Rappolt, M., and G. Rapp. 1996a. Simultaneous small- and wide-angle x-ray diffraction during the main transition of dimyristoylphosphatidylethanolamine. *Ber. Bunsenges. Phys. Chem.* 100:1153–1162

Rappolt, M., and G. Rapp. 1996b. Structure of the stable and metastable ripple phase of dipalmitoylphosphatidylcholine. *Eur. Biophys. J.* 24:381–386.

Ruiz-Argüello, M. B., G. Basáñez, F. M. Goñi, and A. Alonso. 1996. Different effects of enzyme-generated ceramides and diacylglycerols in phospholipid membrane fusion and leakage. *J. Biol. Chem.* 271:26616–26621.

Shah, J., J. M. Atienza, R. I. Duclos, Jr., A. V. Rawlings, Z. Dong, and G. G. Shipley. 1995a. Structural and thermotropic properties of synthetic C16:0 (palmitoyl) ceramide: effect of hydration. *J. Lipid Res.* 36:1936–1944.

Shah, J., J. M. Atienza, A. V. Rawlings, and G. G. Shipley. 1995b. Physical properties of ceramides: effect of fatty acid hydroxylation. *J. Lipid Res.* 36:1945–1955.

Silvius, J. R. 1982. Thermotropic phase transitions of pure lipids in model membranes and their modifications by membrane proteins. *In* Lipid-

Protein Interactions, Vol. 2. P. C. Jost and O. H. Griffith, editors. John Wiley and Sons, New York. 239–281.

Smart, E. J., G. A. Graf, M. A. McNiven, W. C. Sessa, J. A. Engelman, P. E. Scherer, T. Okamoto, and M. P. Lisanti. 1999. Caveolins, liquid-ordered domains, and signal transduction. *Mol. Cell. Biol.* 19:7289–7304.

Thomas, R. L., Jr., C. M. Matsko, M. T. Lotze, and A. A. Amoscato. 1999. Mass spectrometric identification of increased C16 ceramide levels during apoptosis. *J. Biol. Chem.* 274:30580–30588.

Thompson, T. E., M. Allietta, R. E. Brown, M. L. Johnson, and T. W.

Tillack. 1985. Organization of ganglioside GM_1 in phosphatidylcholine bilayers. *Biochim. Biophys. Acta.* 817:229–237.

Voet, D., and J. G. Voet. 1995. Lipid metabolism. *In* Biochemistry. John Wiley and Sons, Somerset, NJ. 662–726.

Weis, R. M. 1991. Fluorescence microscopy of phospholipid monolayer phase transitions. *Chem. Phys. Lipids.* 57:227–239.

Weis, R. M., and H. M. McConnell. 1985. Cholesterol stabilizes the crystal-liquid interface in phospholipid monolayers. *J. Phys. Chem.* 89:4453–4459.